Evaluating INS/GNSS/LiDAR Availability for Self-Driving Cars in Urban Environments

Kana Nagai, Matthew Spenko, Ron Henderson, Boris Pervan, *Illinois Institute of Technology*

BIOGRAPHY

Kana Nagai is currently a Ph.D. candidate and Research Assistant in Mechanical and Aerospace Engineering at Illinois Institute of Technology (IIT). She received her B.S. in Mechanical Engineering from IIT and B.E. in Architecture from Hokkaido University, Japan.

Dr. Matthew Spenko is a Professor of Mechanical and Aerospace Engineering at Illinois Institute of Technology. He earned his B.S. degree in Mechanical Engineering from Northwestern University in 1999 and M.S. and Ph.D. degrees in Mechanical Engineering from the Massachusetts Institute of Technology in 2001 and 2005, respectively. From 2005–2007 he was an Intelligence Community postdoctoral fellow working at Stanford University in the Mechanical Engineering Department.

Ron Henderson FASLA is Professor and Director of the Landscape Architecture + Urbanism Program at Illinois Institute of Technology. He is founding principal of LIRIO Landscape Architecture, Senior Fellow at Dumbarton Oaks, and a Japan-US Creative Fellow. Prof. Henderson received his B.Arch. from University of Notre Dame and his Master of Landscape Architecture and Master of Architecture from University of Pennsylvania.

Dr. Boris Pervan is a Professor of Mechanical and Aerospace Engineering at Illinois Institute of Technology, where he conducts research on advanced navigation systems. Prior to joining the faculty at IIT, he was a spacecraft mission analyst at Hughes Aircraft Company (now Boeing) and a postdoctoral research associate at Stanford University. Prof. Pervan received his B.S. from the University of Notre Dame, M.S. from the California Institute of Technology, and Ph.D. from Stanford University.

ABSTRACT

We evaluate INS/GNSS-based navigation availability against prospective integrity requirements for self-driving cars in urban environments. Specifically, we quantify how long and under what local conditions a practical integrated navigation system, consisting of GNSS, INS, wheel speed sensors, 3-D maps, and vehicle dynamic constraints, can maintain fault-free integrity along a real urban street transect in downtown Chicago. The results show that the integrated system cannot ensure availability across the entire transect, even with four GNSS constellations, and that the main factors influencing unavailable regions are building height, IMU grade, alert limit, and vehicle speed. After the deficient locations are exposed, we consider landmark localization by LiDAR to maintain continuous navigation. We derive ranging error models and investigate placement configurations of pole-like landmarks to ensure availability of INS/GNSS/LiDAR self-driving car fault-free integrity.

I. INTRODUCTION

Global Navigation Satellite Systems (GNSS) provide navigation services globally, but high-rise buildings disturb satellite signal transmissions in urban areas. This leads to a mixture of GNSS-available and -denied environments (Fig. 1). In [1], we evaluated GNSS availability in a real urban environment and determined where it was able to maintain sufficient levels of accuracy and fault-free integrity for self-driving cars.

GNSS signal prediction in urban environments has been conducted in previous work. The concept of 'shadow matching' [2] was developed to identify GNSS signal blockages in urban canyons. Overlaying sky plots on a hemispherical sky view can be used to distinguish between line of sight (LOS) and non-line of sight (NLOS) signals [3]. Reflected rays can be predicted by using Householder transformations [4] to reveal potential multipath conditions.

GNSS alone is generally not able to ensure city-wide availability, so integration with other sensors is needed. Tightly coupled GNSS and inertial navigation systems (INS) using Extended Kalman filter (EKF) integration provide better estimation results [5]. The EKF also enables integration of wheel speed sensors and vehicle dynamic constraints [6] to further improve continuity. However, the performance the integrated system is fundamentally limited by the INS, which drifts over time and cannot ensure continuity of self-driving car integrity through a city under slow driving speeds. [7]. The situation can potentially be improved by means of ranging augmentation using local landmarks, high integrity maps, and light detection and ranging (LiDAR) sensors [8]. Once GNSS/INS-unavailable regions are determined, LiDAR augmentation can be implemented. In this paper, we discuss configurations of pole-like landmarks to maintain continuous navigation with fault-free integrity, and we define ranging error models from these landmarks for this purpose. Our overall goal is to provide tools to help design future urban

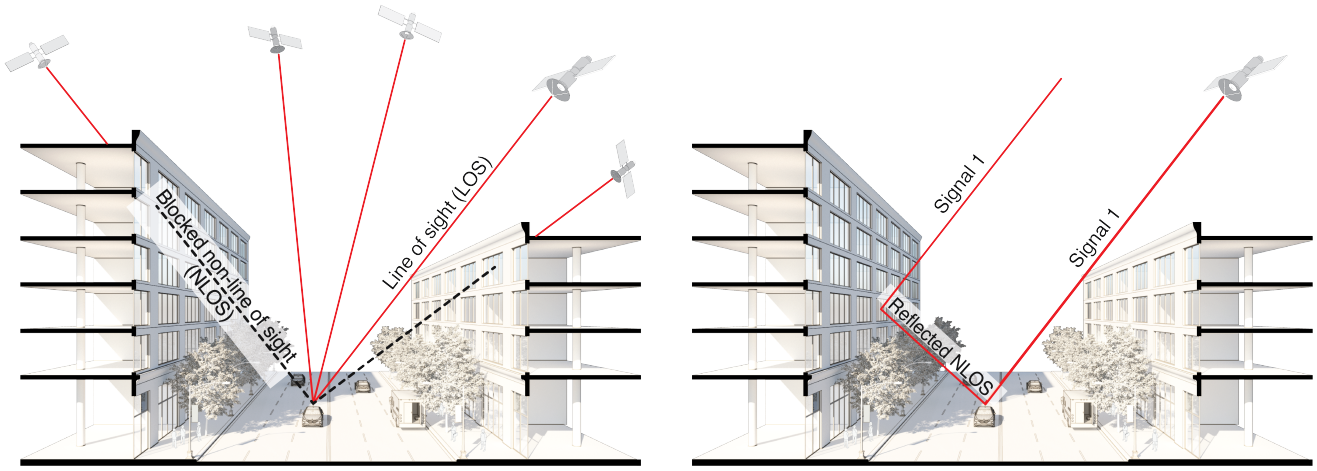

(a) LOS signals and blocked NLOS signals

(b) reflected NLOS signals

Figure 1: The figures depict three types of GNSS signal reception in an urban environment: (a) direct LOS signals and blocked NLOS signals (b) reflected NLOS signals.

environments where people and self-driving cars can safely co-exist.

The remainder of the paper is laid out as follows. Section II introduces navigation performance metrics and integrity requirements for a self-driving car. Section III describes the methods used to evaluate availability of fault-free integrity. Section IV presents the simulation scenario and the urban environment (downtown Chicago) used in the performance simulations. In Section V, we execute the simulations and show the availability results. Section VI describes the LiDAR error model, landmark configurations, and their relations to integrity. Finally, Section VII presents our conclusions.

II. NAVIGATION INTEGRITY CONCEPTS

1. Navigation Performance Metrics

GNSS can resolve vehicle position when the number of visible satellites is greater than three, but the number of satellites alone does not guarantee any specific level of position accuracy. Accuracy is a measure of nominal system error, quantified as standard deviation σ_{pos}, which for GNSS is associated with satellite geometry and ranging error. The geometry in urban environments is generally weak because it is adversely affected by the buildings partially occupying the sky. When the position error exceeds a maximum allowable position error standard deviation, the system should no longer be used for navigation.

In this research, we assume that a fault-free situation defining integrity performance of a system is either 'nominal operations' or 'system unavailable,' and it is specified by a protection level and an alert limit. The horizontal positioning error for a vehicle must be bounded by the protection level computed with the probability that integrity requirements specify. Then, for navigation to be deemed 'available,' the protection level must not exceed a required alert limit. The maximum allowable probability of exceedance and the alert limit can together be used to determine the maximum allowable position error standard deviation. Based on the integrity measure, we evaluate availability as a percentage of time when a system provides navigation service meeting the requirements.

2. Integrity Requirement

We assume that the integrity of a self-driving car requires the probability of exceeding a 0.5-meter alert limit to be lower than 10^{-7} in both along-track (x) and cross-track (y) directions [9]. The 0.5-meter alert limit corresponds to approximately $5\sigma_{\text{pos}}$, so the maximum allowable position error standard deviation is approximately 0.1 m. Accuracy at this level requires differential carrier phase GNSS [10]. The overall integrity requirement assumptions in the paper are organized in Table 1.

Table 1: Self-driving car integrity requirement assumptions

	Direction	Unit	Value
Alert limit	(x, y)	m	(0.5, 0.5)
Probability of allowable exceedance	(x, y)	-	10^{-7}
The max. allowable position error standard deviation	(x, y)	m	(0.1, 0.1)

III. INTEGRITY EVALUATION

1. INS/GNSS-based Navigation System Integrity Evaluation

Tightly coupled INS/GNSS-based integration with an EKF utilizes the INS measurement to predict the vehicle motion [11]. The INS continuous process model is described as

$$\dot{\boldsymbol{x}}_k = \boldsymbol{F}_k \boldsymbol{x}_k + \boldsymbol{G}_{uk} \boldsymbol{u}_k + \boldsymbol{G}_{wk} \boldsymbol{w}_k \tag{1}$$

where $\boldsymbol{x} = [\delta \boldsymbol{r}_N, \delta \boldsymbol{v}_N, \delta \boldsymbol{E}_N, \boldsymbol{b}, \boldsymbol{N}]^T$ is the state vector having position $\boldsymbol{r}$ in the navigation frame, velocity $\boldsymbol{v}$, attitude $\boldsymbol{E}$, bias errors $\boldsymbol{b}$, and cycle ambiguities $\boldsymbol{N}$. $\boldsymbol{u} = [\delta \tilde{\boldsymbol{f}}_B, \delta \tilde{\boldsymbol{\omega}}_B]^T$ is the input vector having accelerometer specific force measurement $\tilde{f}$ in the body frame and gyro rotation rate measurement $\tilde{\omega}$. $\boldsymbol{w} \sim N(0, \boldsymbol{W})$ is the white noise vector of the process model.

The EKF GNSS measurement model is described as

$$\boldsymbol{z}_k = \boldsymbol{H}_k \boldsymbol{x}_k + \boldsymbol{\Gamma}_{vk} \boldsymbol{v}_k \tag{2}$$

where $\boldsymbol{z}$ is the measurement vector having carrier and code phases, and $\boldsymbol{H}$ is the observation matrix containing LOS vectors and excluding the satellites producing blocked and reflected NLOS signals by the procedure in [1]. Some of the signals deemed LOS may produce multipath reflections from nearby buildings that degrade positioning accuracy. We take the multipath interference seriously and exclude all satellites that produce reflected signals detected by Householder transformation. $\boldsymbol{v} \sim (0, \boldsymbol{V})$ is the white noise vector of the receiver.

Wheel speed sensors (WSS) are standard equipment of all vehicles, and vehicle dynamic constraints (VDC) of holonomic and non-holonomic are applicable without any equipment. We developed the model consisting of wheel speed sensor measurement in the along-track direction (v_x), non-holonomic constraint resisting lateral sliding (v_y), and holonomic constraint on vertical movement (v_z) in [7]:

$$\begin{aligned} \boldsymbol{\omega} - \boldsymbol{\omega}^* = {}^B\mathbf{R}^{N*} \delta \boldsymbol{v}_N + ({}^B\mathbf{R}^{N*} \boldsymbol{v}_N^* \times + \boldsymbol{L}_B \, {}^B\mathbf{R}^{N*} \, {}^I\boldsymbol{\omega}_N^E \times) \delta \boldsymbol{E}_N + \boldsymbol{L}_B \mathbf{b}_g \\ + \begin{bmatrix} -\frac{\omega_R}{2} \delta r_R - \frac{\omega_L}{2} \delta r_L \\ 0 \\ 0 \end{bmatrix} - \boldsymbol{L}_B \delta^I \tilde{\boldsymbol{\omega}}_B^B + [\boldsymbol{L}_B \quad \boldsymbol{I}] \, \boldsymbol{v}_\omega \end{aligned} \tag{3}$$

where $\boldsymbol{\omega} = [(\omega_R r_0 + \omega_L r_0)/2, 0, 0]^T$ is the measurement vector of velocity obtained from the wheel speed sensors and vehicle dynamic constraints. The INS/GNSS/WSS/VDC integration using the EKF consists of the process model (1) and the measurement models (2), (3) and is referred to multi-sensor integration in the paper.

We use the state error covariance for the integrity analysis. The EKF error covariance matrix propagation is described as

$$\hat{\boldsymbol{P}}_k = (\mathbf{I} - \boldsymbol{K}_k \boldsymbol{H}_k) \bar{\boldsymbol{P}}_k \tag{4}$$

$$\bar{\boldsymbol{P}}_{k+1} = \boldsymbol{\Phi}_k \hat{\boldsymbol{P}}_k \boldsymbol{\Phi}_k^T + \boldsymbol{Q}_k \tag{5}$$

where $\hat{\boldsymbol{P}}$ is the updated estimate covariance, $\boldsymbol{K}$ is the Kalman gain, $\bar{\boldsymbol{P}}$ is the predicted estimate covariance, $\boldsymbol{\Phi}$ is the state transition matrix, and $\boldsymbol{Q}$ is the covariance associated with $\boldsymbol{w}$ in the discrete time domain. $\bar{\boldsymbol{P}}$ contains each state's error variance along the diagonal:

$$\bar{\boldsymbol{P}} = \begin{bmatrix} \boldsymbol{\Sigma}_r & \bullet & \bullet & \bullet & \bullet \\ \bullet & \boldsymbol{\Sigma}_v & \bullet & \bullet & \bullet \\ \bullet & \bullet & \boldsymbol{\Sigma}_E & \bullet & \bullet \\ \bullet & \bullet & \bullet & \boldsymbol{\Sigma}_b & \bullet \\ \bullet & \bullet & \bullet & \bullet & \boldsymbol{\Sigma}_N \end{bmatrix}. \tag{6}$$

The position error standard deviation contains

$$\boldsymbol{\Sigma}_{pos} = \begin{bmatrix} \sigma_x^2 & \bullet & \bullet \\ \bullet & \sigma_y^2 & \bullet \\ \bullet & \bullet & \sigma_z^2 \end{bmatrix} \tag{7}$$

where σ_x is error standard deviation of along-track (heading), σ_y is that of cross-track (lateral), and σ_z is that of the vertical direction. We compare the σ_x and σ_y to 0.1 m, the maximum allowable position error standard deviation from the integrity requirement in Table 1. $\bar{\boldsymbol{P}}$ is used for integrity evaluation rather than $\hat{\boldsymbol{P}}$ because it will be available to the vehicle at the INS output rate, which will be higher than the GNSS output rate.

2. Availability Evaluation

Integrity at a fixed point changes over time due to GNSS satellite motion, and the evaluation result is valid only for a short period. To quantify the fractional duration of the acceptable performance, we evaluate availability defined as

$$\% = \frac{\text{total time meeting the integrity requirement}}{\text{24 hours}} \times 100. \tag{8}$$

3. INS/LiDAR Integrity Evaluation

INS/GNSS-based navigation accuracy in urban environments is influenced by external factors outside the control of the onboard navigation system. To regain some control over navigation performance, we investigate a potential INS/LiDAR integrated solution. A vehicle equipped with a LiDAR sensor detects objects in its surrounding space and measures the ranges and angles to those with its field of view. Then, the LiDAR data points are associated with pre-defined landmarks on a map. The mapped landmark locations and LiDAR measurements between the vehicle and the landmarks enable the vehicle to estimate its position. The landmark measurements are modelled as

$$d^i = \sqrt{(p_x^i - x_N)^2 + (p_y^i - y_N)^2} + v_d \tag{9}$$

$$\theta^i = \tan^{-1}\left(\frac{p_x^i - x_N}{p_y^i - y_N}\right) - \psi_N + v_\theta \tag{10}$$

where, d^i is ranging measurement of the i^{th} landmark ($i = 1, 2, ..., n$), p_x^i, p_y^i are landmark locations in the navigation frame, x_N, y_N are vehicle positions, v_d is the ranging measurement white noise, θ^i is the angle measurement of the i^{th} landmark, ψ_N is yaw angle, and v_θ is the angle measurement white noise.

The location on the map has some inaccuracy, and the distance from the actual location is called survey error. We introduce landmark locations states (p_x^i and p_y^i) to reflect the error on the estimation. Equations (9) and (10) are linearized for EKF sensor integration:

$$\underbrace{\begin{bmatrix} \boldsymbol{d}^i - \boldsymbol{d}^{i*} \\ \boldsymbol{\theta}^i - \boldsymbol{\theta}^{i*} \end{bmatrix}}_{z_k} = \underbrace{\begin{bmatrix} \boldsymbol{H}_1 & 0 & 0 & 0 & 0 & \boldsymbol{H}_2 \\ \boldsymbol{H}_3 & 0 & \boldsymbol{H}_4 & 0 & 0 & \boldsymbol{H}_5 \end{bmatrix}}_{H_k} \underbrace{\begin{bmatrix} \delta \boldsymbol{r}_N \\ \delta \boldsymbol{v}_N \\ \delta \boldsymbol{E}_N \\ \hline \boldsymbol{b}_a \\ \boldsymbol{b}_g \\ \hline \delta \boldsymbol{p}^i \end{bmatrix}}_{x_k} + \underbrace{\begin{bmatrix} \boldsymbol{v}_d \\ \boldsymbol{v}_\theta \end{bmatrix}}_{v_k} \tag{11}$$

$$\boldsymbol{H}_1 = \begin{bmatrix} \frac{-(p_x^{i*} - x_N^*)}{\sqrt{(p_x^{i*} - x_N^*)^2 + (p_y^{i*} - y_N^*)^2}} \\ \frac{-(p_y^{i*} - y_N^*)}{\sqrt{(p_x^{i*} - x_N^*)^2 + (p_y^{i*} - y_N^*)^2}} \\ 0 \end{bmatrix}^T, \quad \boldsymbol{H}_2 = \begin{bmatrix} \frac{(p_x^{i*} - x_N^*)}{\sqrt{(p_x^{i*} - x_N^*)^2 + (p_y^{i*} - y_N^*)^2}} \\ \frac{(p_y^{i*} - y_N^*)}{\sqrt{(p_x^{i*} - x_N^*)^2 + (p_y^{i*} - y_N^*)^2}} \end{bmatrix}^T$$

$$\boldsymbol{H}_3 = \begin{bmatrix} \frac{-(p_y^{i*} - y_N^*)}{(p_x^{i*} - x_N^*)^2 + (p_y^{i*} - y_N^*)^2} \\ \frac{(p_x^{i} - x_N^*)}{(p_x^{i} - x_N^*)^2 + (p_y^{i} - y_N^*)^2} \\ 0 \end{bmatrix}^T, \boldsymbol{H}_4 = \begin{bmatrix} 0 \\ 0 \\ -1 \end{bmatrix}^T, \boldsymbol{H}_5 = \begin{bmatrix} \frac{(p_y^{i*} - y_N^*)}{(p_x^{i*} - x_N^*)^2 + (p_y^{i*} - y_N^*)^2} \\ \frac{-(p_x^{i*} - x_N^*)}{(p_x^{i*} - x_N^*)^2 + (p_y^{i*} - y_N^*)^2} \\ 0 \end{bmatrix}^T.$$

The INS/LiDAR integration uses the EKF with the process model (1) and the measurement model (11).

IV. SIMULATION SCENARIO

We imagine a future driverless car mission scenario in which the four GNSS constellations consisting of GPS (U.S.), Galileo (E.U.), GLONASS (Russia), and Beidou (China) are present, and multi-sensor navigation systems are practicable. Autonomous vehicles will be held outside the urban core when not in use to minimize congestion in a city. In the open-sky environment, a self-driving car in a parking lot completes differential GNSS initialization, including carrier cycle resolution. Once requested for action, it departs for the urban core, and the subsequent motion of the vehicle with precise GNSS positioning enables INS alignment. Continuity of subsequent navigation can be ensured using the INS under overpasses in the (otherwise) open-sky environment. Upon entering the urban core, the integrated navigation system enables landmark localization by LiDAR.

In (Fig. 2) we prepared a 3D-mapped transect along State Street in Chicago running south to north from low rise neighborhoods to central downtown. A vehicle heads downtown from the low-rise neighborhood through identified open sky environments. After passing through the area, the vehicle enters a middle-rise neighborhood where overpasses disturb GNSS signals. The car keeps driving northward entering the gate of a high-rise neighborhood where skyscrapers taller than 100 m exist. There are 207 evaluation points at approximately 20 m intervals over a total distance of 4 km in the test site. The list of sensor noise parameters are in Table 2.

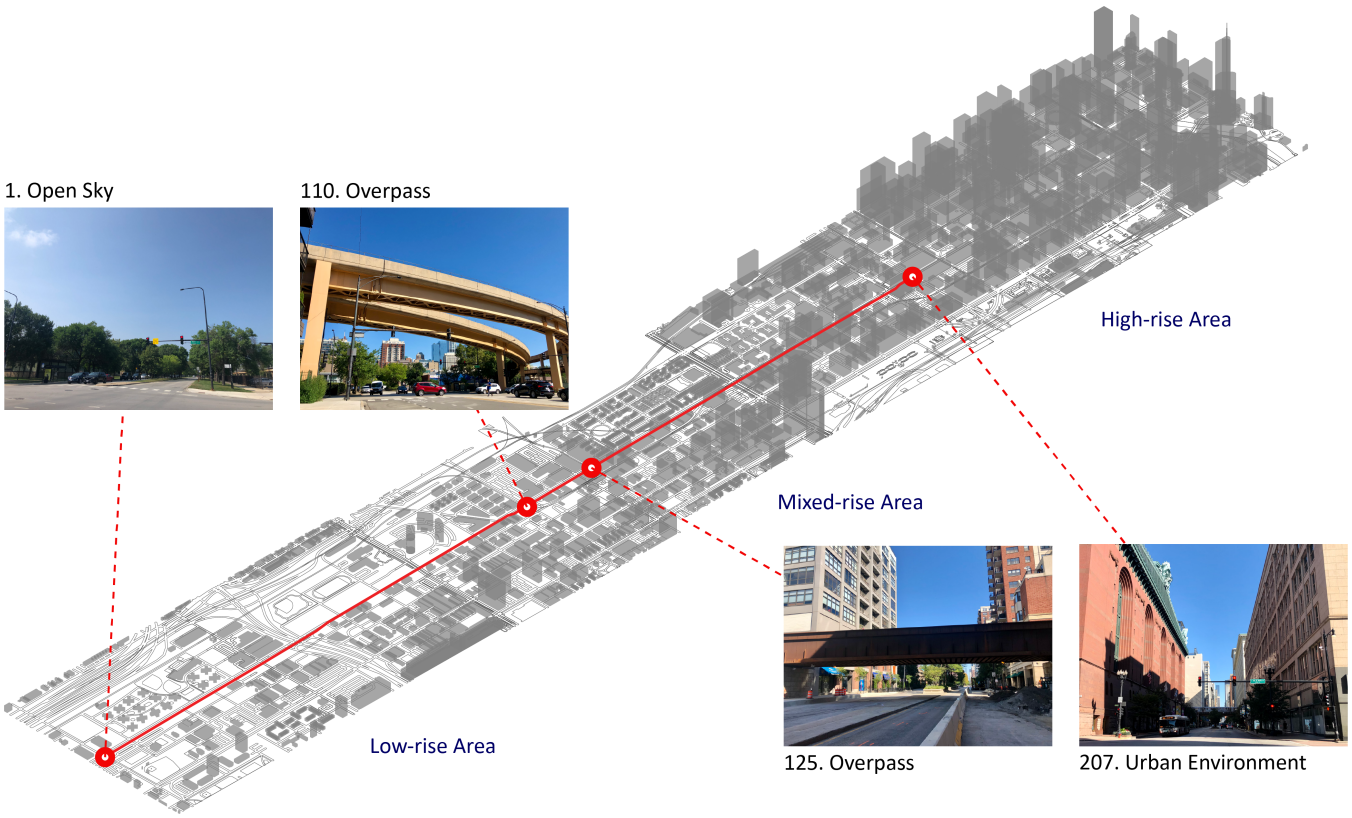

Figure 2: 3D-mapped State Street in Chicago; the street transits from low-rise neighborhoods on the south to central downtown on the north.

Table 2: List of Multi-sensor Noise Parameters

		Unit	Value
GNSS	Carrier Thermal Noise	m	0.001
	Code Thermal Noise	m	0.25
	Carrier Multipath	m	0.005
	Code Multipath	m	0.5
	Multipath Time Constant	s	60
Speed Sensor	Measurement Noise	m	0.05
Holonomic Constraint	Violation Noise	m	0.001
IMU Automotive	Angular random walk	deg/$\sqrt{\text{hr}}$	3
	Gyro Bias Repeatability	deg/hr	1000
	Gyro Bias Stability	deg/hr	100
	Velocity random walk	m/s/$\sqrt{\text{hr}}$	0.12
	Accelerometer Bias Repeatability	mg	100
	Accelerometer Bias Stability	mg	10

V. AVAILABILITY RESULT

1. GNSS-Only Integrity Result

We evaluate GNSS-only integrity by the calculation of the position error standard deviation. Fig. 3 shows the results when we exclude GNSS satellites causing blocked and reflected NLOS signals. The x-axis presents the simulation points corresponding to the side view of the street. The left side is the open sky environment, and the right side is central downtown. The gray bars are the projection of building heights along the street.

As long as the vehicle drives in the open sky environment, the position error standard deviations hold their the initialization values. However, once the vehicle passes under the overpass, all GNSS cycle ambiguities are reset, and the position errors always exceed the maximum allowable position error standard deviation. This result clearly shows that INS is needed in the urban environment.

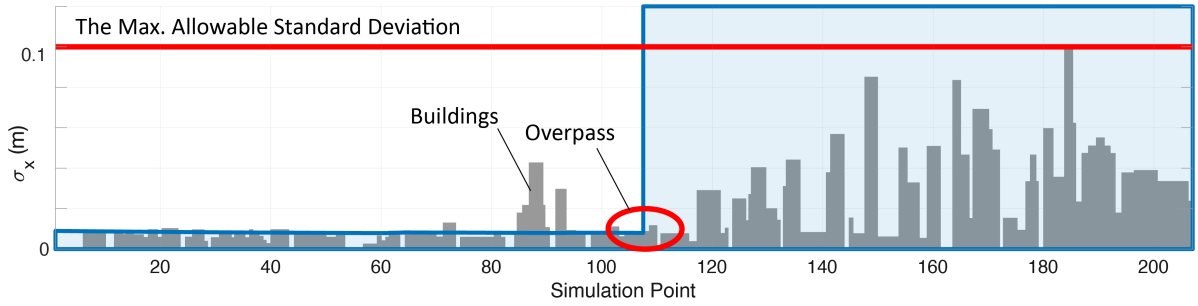

Figure 3: Three cases of GNSS-only availability results

2. INS/GNSS-Based Integrity Result

The multi-sensor integrated navigation system, consisting of INS, GNSS, wheel speed sensors (WSS), and vehicle dynamic constraints (VDC), can improve navigation availability. We evaluate the multi-sensor navigation integrity with (7) when a self-driving car leaves for the downtown from the open-sky environment at midnight or midday. Example results are shown in Fig. 4. Since the INS keeps tracking position without GNSS measurement updates, the cycle ambiguities are bridged at overpasses. The environment is the prime factor influencing navigation integrity, and when the vehicle goes through dense urban areas, the maximum allowable position error standard deviation is exceeded. Timing is another factor, and the number of points exceeding varies between midnight and midday due to GNSS satellite motion. Integrity is affected not only by building height but time of day. Availability needs to be examined over the entire day to determine outage durations.

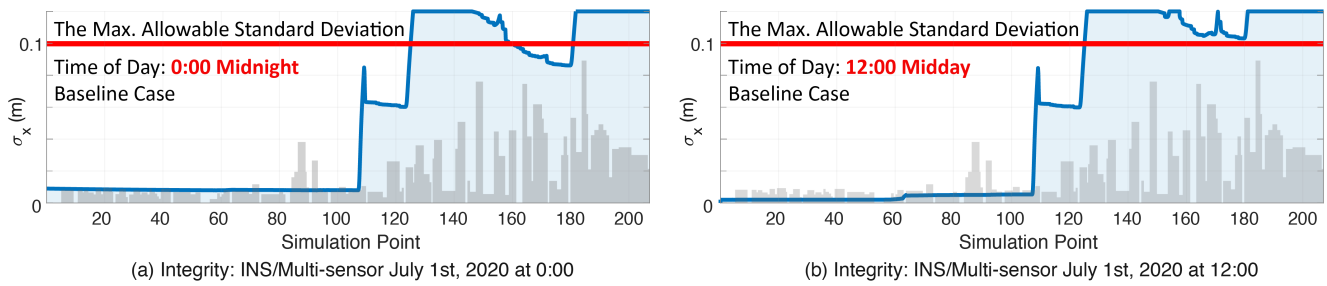

(a) Integrity: INS/Multi-sensor July 1st, 2020 at 0:00

(b) Integrity: INS/Multi-sensor July 1st, 2020 at 12:00

Figure 4: Integrity simulation: the multi-sensor position error at times of day

3. INS/GNSS-Based Availability Result

We evaluate availability when a car starts driving from simulation point 1 toward 207 every 2 minutes over 24 hours and determine the fraction of time at each point when the horizontal position error standard deviations are less than 0.1 m. Availability of the multi-sensor integration is exhibited in Fig. 5 for a baseline case defined in Table 3: four GNSS constellations are used, excluding satellites causing blocked and reflected NLOS, together with an automotive-grade IMU. The alert limit is 0.5 m, and the car travels at a constant velocity of 5 m/s. When the system is operated over 24 hours, the availability should be 100 percent. The Gantt charts in Fig. 5 visualize the percentage by white (100 percent) and black (less than 100 percent), and 'Acceptance' means the point reaches 100-percent in both x and y directions.

Since the availability varies with IMU grade, sensor equipage, alert limit, and vehicle speed, we conduct a sensitivity analysis by comparing specific cases with the baseline. The purpose is to know how long and under what local conditions a vehicle's navigation protection level does not exceed an alert limit with the multi-sensor navigation system.

Table 3: Sensitivity analysis cases ('-' stands for the same as the baseline case)

	Baseline	IMU Grade	Sensor	Alert Limit	Speed
IMU Grade	Automotive	Tactical	-	-	-
Sensor	INS/Multi.	-	INS/GNSS	-	-
Alert Limit	(0.5 m, 0.5 m)	-	-	(1.0 m, 0.7 m)	-
Speed	5 m/s	-	-	-	10 m/s
Figure	Fig. 5	Fig. 6	Fig. 7	Fig. 9	Fig. 10

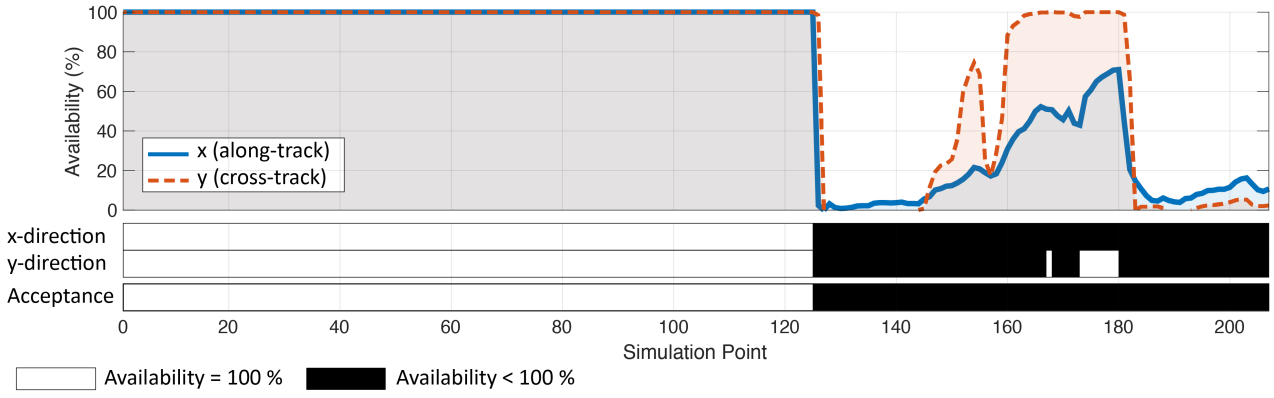

Figure 5: Availability simulation at the baseline case

a). IMU Grade

An automotive-grade IMU is cost-friendly and a realistic option for economy cars at this moment. STIM300 is a tactical grade IMU that provides better performance but also comes at a high price. Random walk, bias repeatability, and bias stability are the main noise sources determining IMU performance. Table 4 exhibits the parameters the simulation uses. The upgraded IMU extends availability significantly (Fig. 6).

Table 4: Random walk, bias repeatability, and stability at each IMU grade

	Unit	Automotive [12]	Tactical (STIM300) [13]
Angular random walk	deg/$\sqrt{\text{hr}}$	3	0.15
Gyro Bias Repeatability	deg/hr	1000	4.0
Gyro Bias Stability	deg/hr	100	0.3
Velocity random walk	m/s/$\sqrt{\text{hr}}$	0.12	0.07
Accelerometer Bias Repeatability	mg	100	0.75
Accelerometer Bias Stability	mg	10	0.05

Analysis	IMU Grade
IMU Grade	Tactical
Sensor	INS/Multi.
Alert Limit	(0.5 m, 0.5 m)
Speed	5 m/s

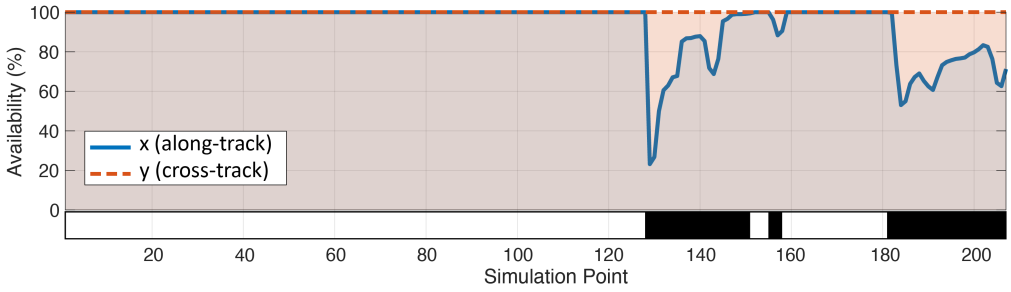

Figure 6: Availability simulation: IMU tactical grade

b). Sensor Equipage

The availability results in Fig. 7 show the INS/GNSS navigation system, which is without the wheel speed sensors (applied to along-track) and vehicle dynamic constraints (applied to cross-track). The INS/GNSS debases availability.

Analysis	Sensor
IMU Grade	Auto.
Sensor	INS/GNSS
Alert Limit	(0.5 m, 0.5 m)
Speed	5 m/s

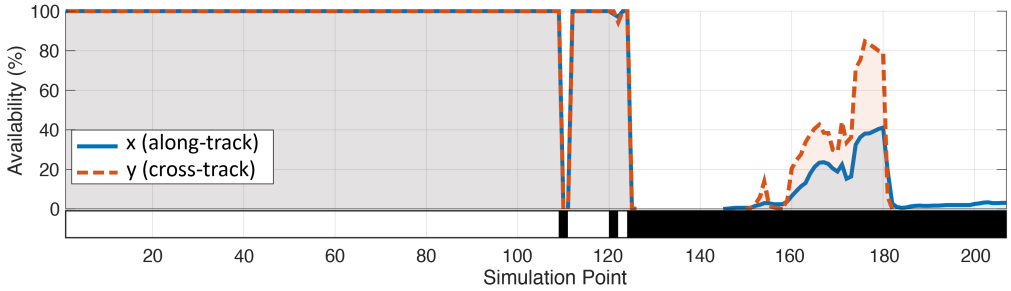

Figure 7: Availability simulation: INS/GNSS sensor

c). Alert Limit

Our assumption of the alert limit is 0.5 m in both x and y directions based on the acceptable limits for a turning vehicle, but an integrity requirement at straight-line motion becomes more relaxed because of the loosened alert limit. According to [9], the alert limits can be defined as

$$X = \sqrt{(r + \frac{w}{2})^2 - (\frac{Y}{2})^2} + \frac{w}{2} - r \tag{12}$$

$$\text{Lateral Alert Limit } = (X - w_v)/2 \tag{13}$$

$$\text{Longitudinal Alert Limit } = (Y - l_v)/2. \tag{14}$$

where w is lane width, r is lane radius, and w_v, w_l are vehicle dimensions. Fig. 8 shows the relationship between lateral and longitudinal alert limits calculated using these equations, and the parameters are in Table 5. For straight-line motion, we choose the 1-meter alert limit in the longitudinal direction and 0.7-meter in the lateral. The loosened integrity requirements make more areas available for navigation (Fig. 9).

Table 5: Self-driving car integrity requirement assumptions

	Notation	Unit	Turning	Straight
Lane Width	w	m	3.4	3.4
Lane Radius	r	m	10	1000
Vehicle Width, Length	(w_v, l_v)	m	(1.94, 5.15)	(1.94, 5.15)
Alert limit	(x, y)	m	(0.5, 0.5)	(1.0, 0.7)
Probability of allowable exceedance	-	-	10^{-7}	10^{-7}
The max. allowable position error standard deviation	(σ_x, σ_y)	m	(0.10, 0.10)	(0.20, 0.14)

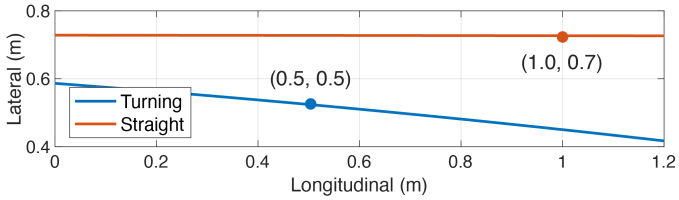

Figure 8: The relationships between lateral alert limit and longitudinal alert limit

Analysis	Alert Limit
IMU Grade	Auto.
Sensor	INS/Multi.
Alert Limit	(1.0 m, 0.7 m)
Speed	5 m/s

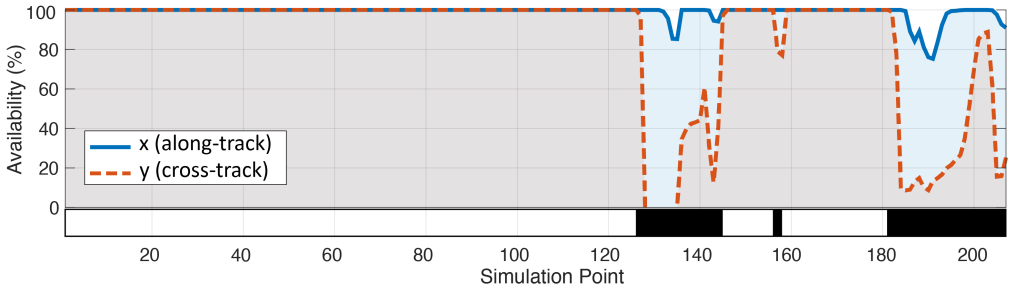

Figure 9: Availability simulation: alert limit at straight motion

d). Vehicle Speed

Our prior research in [7] showed that INS/GPS position errors along a path depended strongly on the vehicle speed. Given this information, we evaluate availability when a vehicle is moving at a constant velocity of 5 m/s (i.e., 18 km/h, 11 mph) or 10 m/s (i.e., 36 km/h, 22 mph) in Fig. 10. The accuracy of the high-speed vehicle is better than that of the slow speed because when a car goes through a GNSS-denied area quickly, the time when the INS error drifts becomes shorter.

Analysis	Speed
IMU Grade	Auto.
Sensor	INS/Multi.
Alert Limit	(0.5 m, 0.5 m)
Speed	10 m/s

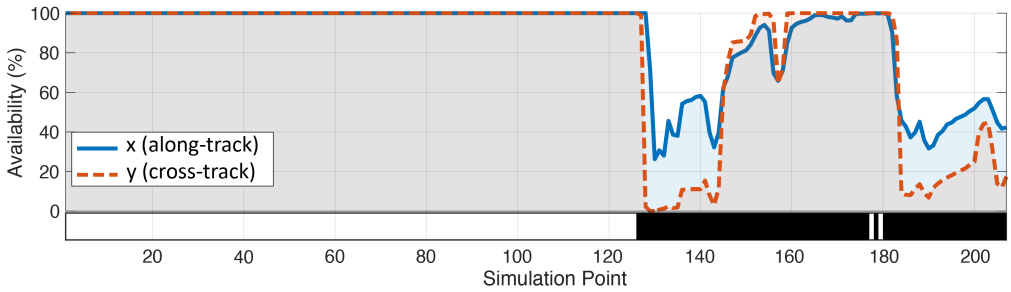

Figure 10: Availability simulation: vehicle speed v = 10 m/s

e). Analysis

We have developed a tool to ascertain the GNSS-based navigation available areas by applying integrity concepts and discussed the factors extending or narrowing them. Fig. 11 summarizes the points where availability reaches 100 percent along the street transect. The figure is categorized by sensors, alert limit, and vehicle speed to compare easily, and the same color means the

same case, with only the INS quality being different.

If a car drives in an open environment, the INS/GNSS-based navigation system maintains availability. However, it does not reach 100 percent everywhere once the car enters the city. The available regions vary with the case, and the coverage ranges from 58 to 100 percent. Speed sensors and dynamic constraints extend the availability for any grade IMUs, so we recommend their integration. Relaxed alert limits, high-speed, and a tactical grade IMU improve availability.

INS/GNSS-based navigation availability is determined by not only building heights but other complex factors. The alert limit is determined by road width and vehicle dimensions. Position errors along a path depend strongly on speed, but a vehicle is unlikely to move at the speed limit in a congested city. In contrast, with these issues, IMU choice is the main user-controllable factor, so in future work, we plan to evaluate which IMU error parameters have particular influence in urban environments. We will also examine availability when the car stops at traffic light and zero-velocity measurement updates can be exploited.

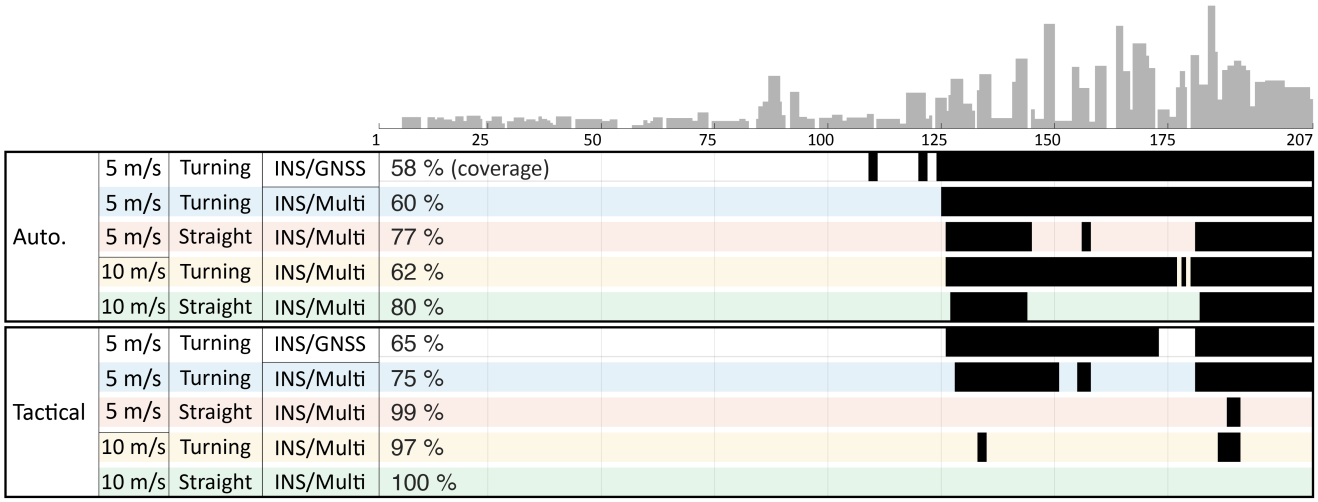

Figure 11: Summary of availability acceptance

VI. INS/LIDAR INTEGRITY

1. Overview

In clear sky areas, GNSS measurements are the only sources needed for positioning and controlling INS drift. Once a vehicle enters an urban core where the number of clear (unreflected) GNSS signals becomes deficient, the positioning and INS drift control burden will be shared with LiDAR landmark measurements. All objects in urban environments are candidates for external ranging sources for LiDAR, but we specifically focus on extracting pole-like landmarks (e.g., trees and street lamps) because of their location flexibility, relative ubiquity, and defined shapes. Prior research showed that LiDAR measurements using pole-like landmarks improved vehicle localization in urban environments but that "the accuracy of the localization is highly dependent on the number and density of available landmarks at each scene" [8]. Given that both the quantities and configurations of pole-like landmarks affect positioning performance, we ask how the number and locations of the landmarks would best be modified to maintain fault-free integrity for self-driving cars. The landmark locations should therefore be arranged with some consideration toward this goal, which is the main motivation of this section.

2. Survey Error Analysis

We carefully construct a new LiDAR measurement error model to accurately estimate positions with the EKF integration. The sources of ranging inaccuracy for these landmarks are present in the form of measurement noise and survey error. Measurement noise is defined by device specification. We use a standard deviation for the LiDAR ranging measurement white noise ($\boldsymbol{v}_d$) of 0.01 m and 0.3 degrees for the angle measurement white noise ($\boldsymbol{v}_\theta$) [14].

Survey error occurs when the mapped center is defined but there is a fixed bias vector discrepancy between the mapped information and the actual center. We include survey error states in the EKF and simulate the impact on the position accuracy. Some details and results of an illustrative covariance analysis are shown in Fig. 12. Sub-figure (c) shows covariance analysis results using (11) (Fig. 12 (b)). The steady-state position error standard deviation is 0.14 m given a 0.2 m standard deviation of survey error (initial value assumption) and 0.015 m given 0.02 m assumption (initial value) under completed alignment. Survey

error directly affects the position estimation of a vehicle. The results show some observability of the survey error through the EKF, but in the simulation knowledge of user position is assumed to be good at 0.02 m standard deviation. In general, survey error will largely translate directly into ranging error.

For many LiDAR applications these differences may be of minor significance, but in our current application centimeter-level errors matter a great deal, and they need to be carefully accounted for in the estimator to ensure integrity.

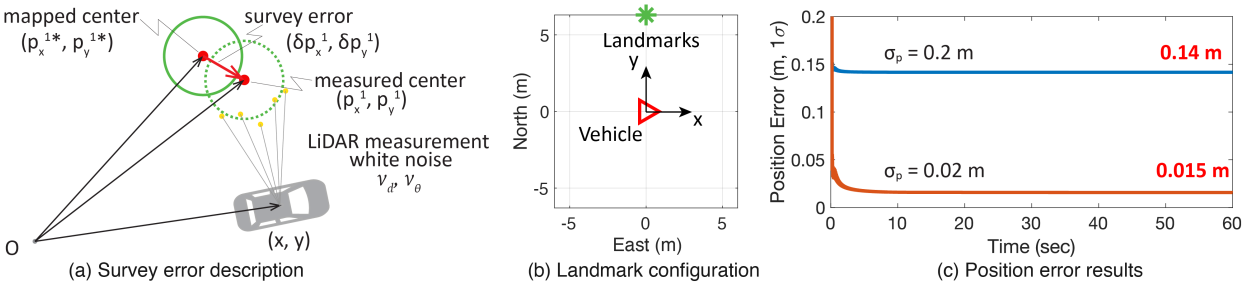

Figure 12: Survey error: (a) the description, (b) configuration of the simulation, and (c) the simulation results

3. Landmark Configuration Analysis

We consider a simple scenario to illustrate the effect of landmark configuration. There are two landmarks and a stationary vehicle. The landmarks are placed 6 m west of the vehicle, and the distance d between them along the north direction is variable (Fig. 13 (a)). Fig. 13 (b) shows the position accuracy given a yaw angle alignment error standard deviation of 1 deg. It is clear that the vehicle can estimate a more accurate position if two landmarks are further apart.

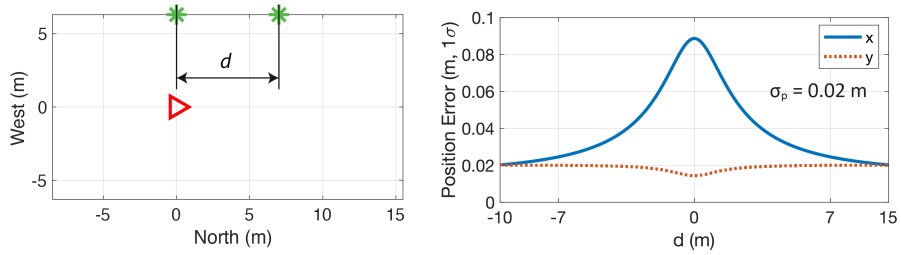

Figure 13: INS/LiDAR position error: (a) configuration of the simulation, and (b) position accuracy

In future work, we will utilize the configuration analysis to help rearrange landmarks within State Street. For example, Fig. 6 shows the availability for the baseline scenario, which showed clear deficiencies after simulation point 125. Through simulations, we will perform a complete analysis on how landmark distancing and positioning within these areas will help improve the availability and the position accuracy of self-driving cars.

VII. CONCLUSION

Using GNSS in urban environments can result in integrity problems for self-driving cars because high-rise buildings disturb the signals. To assess the performance of practical integrated navigation systems (i.e. GNSS, INS, wheel speed sensors, 3-D maps, and vehicle dynamic constraints) in various environments, we determined where the systems were able to maintain fault-free integrity in an example Chicago street: State Street. The availability of the system (i.e. the fractional duration of the integrity) was then computed. The results showed that the availability depended on a number of factors, including high-rise buildings, IMU grade, integrity requirements, and vehicle speed. Also, several areas of the street did not reach 100% availability, meaning continuous navigation in these areas would be challenging. To cope with that, landmark positioning by LiDAR was considered. A new LiDAR measurement error model was derived and various configurations of pole-like landmarks were examined in terms of their impact on vehicle position accuracy.

In future work, we will perform a sensitivity analysis to determine which IMU noise parameters influence the most the position error drift in urban environments. We will also analysis the system's availability when a self-driving car stops at traffic lights. In parallel, the study of landmark configurations will be consolidated to analyse which configurations can maintain integrity for

self-driving cars throughout the entire city.

ACKNOWLEDGEMENTS

This research is supported by the National Science Foundation (Grant No. 1830642).

Fig. 1 and the 3D maps were created by Alexis Arias, Landscape Architecture + Urbanism, IIT. The authors greatly appreciate the advice and help of Nilay Mistry, Landscape Architecture + Urbanism.

REFERENCES

[1] K. Nagai, T. Fasoro, M. Spenko, R. Henderson, and B. Pervan, "Evaluating GNSS navigation availability in 3-D mapped urban environments," *2020 IEEE/ION Position, Location and Navigation Symposium, PLANS 2020*, pp. 639–646, 2020.

[2] P. D. Groves, "Shadow matching: A new GNSS positioning technique for urban canyons," *Journal of Navigation*, vol. 64, no. 3, pp. 417–430, 2011.

[3] L. Chapman, J. E. Thornes, and A. V. Bradley, "Sky-view factor approximation using GPS receivers," *International Journal of Climatology*, vol. 22, no. 5, pp. 615–621, 2002.

[4] A. S. Householder, "Unitary triangularization of a nonsymmetric matrix," *Journal of the ACM (JACM)*, vol. 5, no. 4, pp. 339–342, 1958.

[5] G. Falco, M. Pini, and G. Marucco, "Loose and tight GNSS/INS integrations: comparison of performance assessed in real urban scenarios," *Sensors (Switzerland)*, vol. 17, no. 2, 2017.

[6] J. Gao, M. G. Petovello, and M. E. Cannon, "Development of precise GPS/INS/wheel speed sensor/yaw rate sensor integrated vehicular positioning system," *Proceedings of the Institute of Navigation, National Technical Meeting*, vol. 2, no. January, pp. 780–792, 2006.

[7] K. Nagai, M. Spenko, R. Henderson, and B. Pervan, "Evaluating INS/GNSS availability for self-driving cars in urban environments," *Proceedings of the 2021 International Technical Meeting of The Institute of Navigation*, pp. 243–253, 2021.

[8] C. Brenner, "Global Localization of Vehicles Using Local Pole Patterns," *Lecture Notes in Computer Science*, pp. 61–70, 2009.

[9] T. G. Reid, S. E. Houts, R. Cammarata, G. Mills, S. Agarwal, A. Vora, and G. Pandey, "Localization requirements for autonomous vehicles," *SAE International Journal of Connected and Automated Vehicles*, vol. 2, no. 3, pp. 1–16, 2019.

[10] P. K. Enge, *The global positioning system: Signals, measurements, and performance*. Springer, 1994, vol. 1, no. 2.

[11] C. Tanil, "Detecting GNSS spoofing attacks using INS coupling," Ph.D. dissertation, Illinois Institute of Technology, 2016.

[12] R. Brown and P. Hwang, *Introduction to Random Signals and Applied Kalman Filtering with Matlab Exercises*. Wiley, 2012.

[13] "STIM300." Accessed Jul. 17, 2021. [Online]. Available: https://www.sensonor.com/products/inertial-measurement-units/stim300/

[14] "Velodyne Puck Lidar Sensor." Accessed Jul. 17, 2021. [Online]. Available: https://velodynelidar.com/products/puck/